JOURNAL OF GEOPHYSICAL RESEARCH, VOL. 113, A03208, doi:10.1029/2007JA012800, 2008

Two-stage oscillatory response of the magnetopause to a tangential discontinuity/vortex sheet followed by northward IMF: Cluster observations

C. J. Farrugia,[1,2] F. T. Gratton,[3,4] E. J. Lund,[1] P. E. Sandholt,[5] S. W. H. Cowley,[6] R. B. Torbert,[1,2] G. Gnavi,[3] I. R. Mann,[7] L. Bilbao,[3] C. Mouikis,[1] L. Kistler,[1,2] C. W. Smith,[1] H. J. Singer,[8] and J. F. Watermann[9]

Received 6 September 2007; revised 23 November 2007; accepted 10 December 2007; published 19 March 2008.

[1] We discuss the motion and structure of the magnetopause/boundary layer observed by Cluster in response to a joint tangential discontinuity/vortex sheet (TD/VS) observed by the Advanced Composition Explorer spacecraft on 7 December 2000. The observations are then supplemented by theory. Sharp polarity reversals in the east-west components of the field and flow B_y and V_y occurred at the discontinuity. These rotations were followed by a period of strongly northward interplanetary magnetic field (IMF). These two factors elicited a two-stage response at the magnetopause, as observed by Cluster situated in the boundary layer at the duskside terminator. First, the magnetopause suffered a large deformation from its equilibrium position, with large-amplitude oscillations of ~3-min period being set up. These are argued to be mainly the result of tangential stresses associated with ΔV_y the contribution of dynamic pressure changes being small in comparison. This strengthens recent evidence of the importance to magnetospheric dynamics of changes in azimuthal solar wind flow. The TD/VS impact caused a global response seen by ground magnetometers in a magnetic local time range spanning at least 12 h. The response monitored on ground magnetometers is similar to that brought about by magnetopause motions driven by dynamic pressure changes. Second, Cluster recorded higher-frequency waves (~79 s). Two clear phases could be distinguished from the spectral power density, which decreased by a factor of ~3 in the second phase. Applying compressible linearized MHD theory, we show that these waves are generated by the Kelvin-Helmholtz (KH) instability. Varying the local magnetic shear at the Cluster locale, as suggested by the temporal profile of the IMF clock angle, we find that locally stability was reinstated, so that the reduced power in the second phase is argued to be due residual KH activity arriving from locations farther to the dayside.

Citation: Farrugia, C. J., et al. (2008), Two-stage oscillatory response of the magnetopause to a tangential discontinuity/vortex sheet followed by northward IMF: Cluster observations, *J. Geophys. Res.*, *113*, A03208, doi:10.1029/2007JA012800.

1. Introduction

[2] The terrestrial magnetopause and its boundary layers are hardly ever at rest. Perhaps the most basic interplanetary parameter responsible for these motions is the dynamic pressure P_{dyn}, a quantity which can vary over two orders of magnitude, compressing and deflating the magnetosphere cavity as it changes. The compressional MHD waves launched into the cavity by these magnetopause motions, and the way they couple to field-guided Alfvèn waves on resonant L shells inside the magnetosphere, thereby transferring momentum to the ionosphere through the field-aligned currents, has been observed and modeled [see, e.g., *Kivelson and Southwood*, 1986; *Farrugia et al.*, 1989; *Freeman et al.*, 1990; *Southwood and Kivelson*, 1990]. Another cause are local instabilities generated at the boundary. The most common of these is the Kelvin-

[1]Space Science Center, University of New Hampshire, Durham, New Hampshire, USA.
[2]Also at Department of Physics, University of New Hampshire, Durham, New Hampshire, USA.
[3]Instituto de Fisica del Plasma, CONICET and Universidad de Buenos Aires, Buenos Aires, Argentina.
[4]Departamento de la Fisica, Pontificia Universidad Catolica Argentina, Buenos Aires, Argentina.
[5]Department of Physics, University of Oslo, Oslo, Norway.
[6]Department of Physics and Astronomy, University of Leicester, Leicester, UK.
[7]Avadh Bhatia Physics Laboratory, Department of Physics, University of Alberta, Edmonton, Canada.
[8]NOAA Space Environment Center, Boulder, Colorado, USA.
[9]Geomagnetism and Space Physics Program, Danish Meteorological Institute, Kobenhavn, Denmark.

0148-0227/08/2007JA012800$09.00

Helmholtz instability feeding on the flow shears which exist across the magnetosheath/magnetosphere interface. Ever since *Dungey* [1955] pointed out the possibility of the magnetopause going Kelvin-Helmholtz unstable, many studies have been devoted to this instability, the surface waves it causes, their coupling to the geomagnetic field giving rise to field line resonances, and how this instability might mediate the entry of magnetosheath plasma into the magnetosphere [e.g., *Southwood*, 1979; *Miura*, 1984; *Chen et al.*, 1993; *Kivelson and Chen*, 1995; *Seon et al.*, 1995; *Fairfield et al.*, 2000; *Otto and Fairfield*, 2000; *Farrugia et al.*, 2000, 2001; *Gratton et al.*, 2004].

[3] Attention has been drawn to two other interplanetary parameters whose changes may occasion considerable deformation and motion of the magnetopause. One is a variable orientation of the interplanetary magnetic field (IMF). *Fairfield et al.* [1990] showed that even when $P_{\rm dyn}$ is constant, the magnetopause and inner magnetospheric boundaries may be in motion. They attributed these motions to pressure changes generated in the foreshock region by the IMF changes. These pressure changes subsequently convect through the bow shock and impinge on the magnetopause. The authors thus concluded that "even in the presence of a solar wind that is absolutely steady in velocity and density but which carries an embedded interplanetary magnetic field of variable orientation, there will be a variation of pressure exerted on the magnetopause." Continuing this line of research, *Laakso et al.* [1998] studied oscillations of the magnetopause during a period of enhanced IMF fluctuations ahead of the 10 January 1997 magnetic cloud and concluded that they were due to rapid changes in the IMF direction. Their analysis suggested that the key parameter was the angle between the bow shock normal and the direction of the upstream IMF θ_{Bn}. This angle varies along the bow shock surface and it is that part of the magnetopause/boundary layer which lies behind the quasi-parallel bow shock that was found to be affected by changes in magnetosheath pressure.

[4] Recently, it has been pointed out that changes in the east-west component of the solar wind velocity V_y may serve as trigger of large motions of magnetospheric structures. Thus *Zong et al.* [2004] considered a case where a 60 km s^{-1} change in V_y from east (positive) to west caused the cusp to swing past Cluster. The authors argued that the back-and-forth motions of the cusp was a temporal change. Both the dynamic pressure as well as the polarity of IMF B_y (the latter being a well-known quantity affecting the location of the cusp [*Newell et al.*, 1989; *Moen et al.*, 1999]) were constant in their example. Further evidence for the control of the polar cusp by IMF V_y was given by *Lundin et al.* [2001].

[5] The aim of this work is to study an example where both field and flow vectors undergo simultaneous, abrupt changes. The interplanetary structure is a combined current and a vortex sheet at which GSM B_y and V_y rotate sharply from west to east. The dynamic pressure changes little across this discontinuity. Specifically, we shall find that compared to $\Delta P_{\rm dyn}$, ΔV_y plays a dominant role in causing the magnetopause to move. A further interesting feature is that the IMF turned strongly northward soon after the discontinuity. This opens the possibility of exciting Kelvin-Helmholtz (KH) waves at the magnetopause. We find this to be indeed the case. In this part of the work we are in the fortunate position of being able to set the boundary conditions for the theoretical analysis with little ambiguity; the earlier, large-amplitude oscillations caused Cluster to sample the magnetosheath and the magnetosphere minutes before the KH waves were observed, so that the parameters of these two regions observed during the oscillations can be used as input to the local KH instability calculations.

[6] We shall see that the two different "triggers" mentioned above, i.e., ΔV_y and northward IMF, which are well separated in time in the interplanetary medium, gave rise to large and clear effects at the magnetopause. However, the onset of the effect due to the second cause might have been advanced by the presence of the first, hastening the development of the instability.

2. Interplanetary Observations: Advanced Composition Explorer

[7] For the 2-h interval 12:00–14:00 UT on 7 December 2000, Figure 1 shows plasma [*McComas et al.*, 1998] and magnetic field [*Smith et al.*, 1998] observations from the Advanced Composition Explorer (ACE) spacecraft in orbit around the Lagrangian L1 point. Figure 1 shows from top to bottom: the proton density, bulk speed, temperature, dynamic pressure, total magnetic field strength, components (pairwise) of the magnetic field and flow vectors in GSM coordinates, and IMF clock angle, i.e., the polar angle in the GSM *Y-Z* plane. The temporal resolutions are 16 s (magnetic field) and 64 s (plasma). The observations refer to a dense solar wind of slightly above average bulk speed in which is embedded an interplanetary magnetic field of slightly above average strength. A prominent feature, highlighted in the eighth and ninth panels, is the eastward (y) rotations in the field and flow occurring at ~12:47 UT. Here IMF B_y reverses polarity from −8 nT to 7 nT, while the flow V_y changes from −40 km s^{-1} west to 25 km s^{-1} east. There are also smaller changes in the other components of the field and flow vectors. The change in the magnetic field direction occurs under constant field strength, while that in the flow direction is accompanied by a small increase in flow speed (from 440 to 460 km s^{-1}). Averaging over 5-min intervals on either side of the discontinuity, we have that the density and bulk speed increase at the time (from 11.56 ± 0.39 cm^{-3} to 12.49 ± 0.30 cm^{-3} and from 436.3 ± 1.0 to 453 ± 7.1 km s^{-1}, respectively), leading to a small increase in the dynamic pressure (fourth panel) of ~17% (from 3.68 ± 0.13 to 4.30 ± 0.15 nPa). At the discontinuity, the IMF turns north, and a few minutes later the clock angle α is for ~9 min very small (~10° on average in 12:53–13:01 UT).

[8] We next discuss the nature of the discontinuity. We carried out a minimum variance analysis [*Sonnerup and Cahill*, 1967] on the magnetic field data in the interval 12:40–13:05 UT. The routine picks out a reliable normal (ratio of intermediate-to-minimum eigenvalues, R = 6.4) with a normal component $B_k \equiv B_n$ = 0.24 ± 1.06 nT consistent with zero, indicating that the field discontinuity is tangential. The data in the interval examined is rotated to these principal axes coordinates and plotted in Figure 2. The first and second panels reproduce the total field and clock angle α for reference, followed by the static pressures (proton and electron (P_p) in blue, magnetic (P_m) in red,

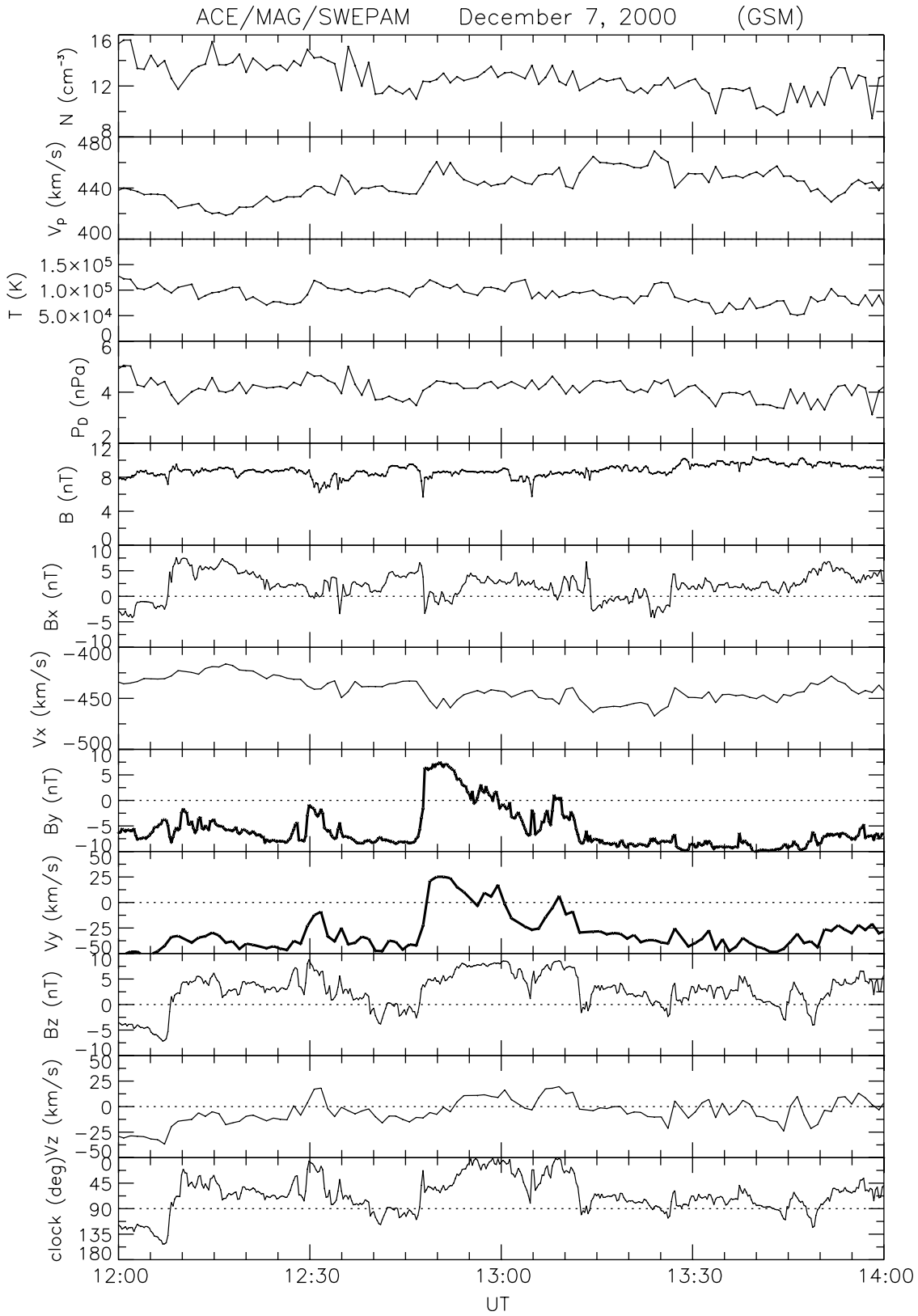

Figure 1. Plasma and magnetic field data from the ACE spacecraft for the period 12:00–14:00 UT on 7 December 2000. From top to bottom: proton density, bulk speed, temperature, dynamic pressure, total field strength, field and flow components (pairwise) in GSM coordinates, and the IMF clock angle. Highlighted in the eighth and ninth panels are the east-west components of the magnetic field and plasma flow velocity.

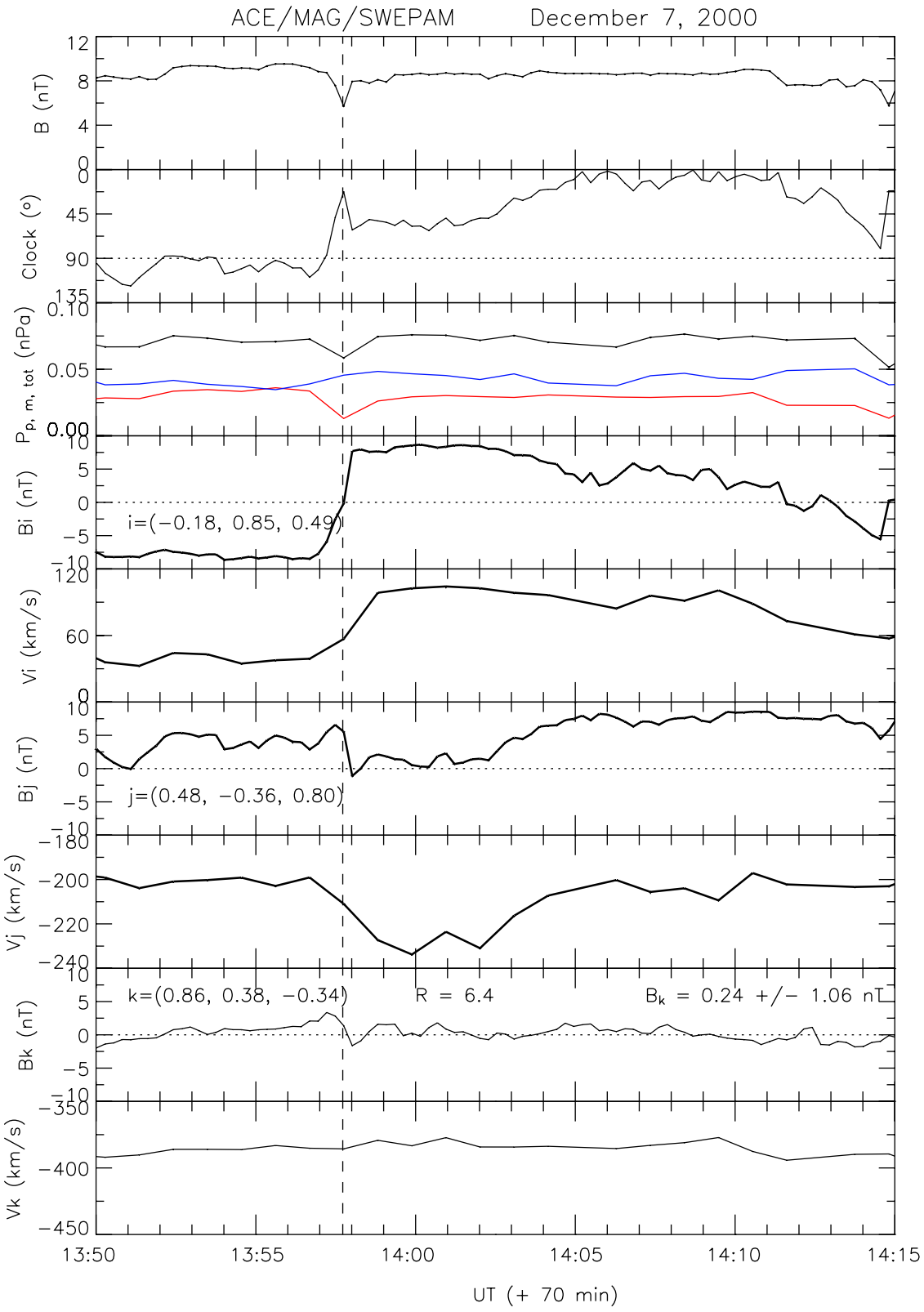

Figure 2. The 25-min interval 13:55–14:15 UT of ACE data plotted in principal axes coordinates (i, j, k). Unit vector **k** is normal to the plane. With respect to Figure 1, the data have been shifted by an estimated 70-min propagation delay from ACE to Cluster. The GSM coordinates of the unit vectors are shown in the B_i, B_j, B_k panels. From top to bottom: the total field; clock angle; thermal pressure, assuming $T_e = T_p$ (blue), magnetic pressure (red), and their sum; and components of the field and flow around the discontinuity.

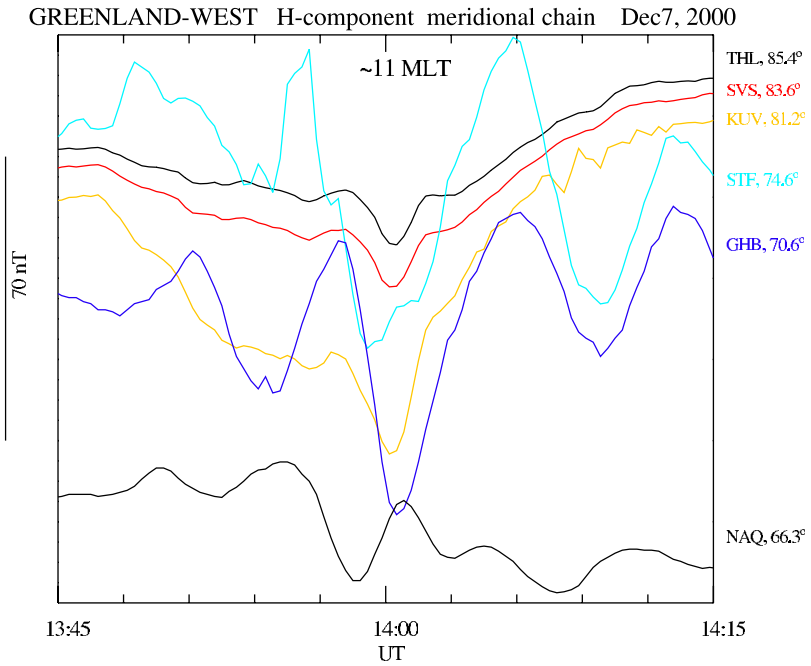

Figure 3. Readings of the horizontal component of the geomagnetic field recorded by six stations of the Greenland-West chain located at ~11:00 MLT.

and their sum (P_{tot})) and the field and flow components. Since electron parameters are not available, to derive the electron pressure, we assumed quasi neutrality and $T_e = T_p$. The normal vector $\mathbf{k} \equiv \mathbf{n}$ = (0.86, 0.38, −0.34) points sunward, duskward, and southward. To anticipate, on impinging on the bow shock, the low-latitude duskside magnetosheath would be behind a quasi-perpendicular shock, while the low-latitude dawnside magnetosheath would be predominantly behind a quasi-parallel shock. There are also substantial changes in the flow components tangential to the plane ($V_{i,j}$). In summary, ACE is observing a current sheet which is simultaneously a vortex sheet. Below we shall estimate the forces exerted on the magnetopause by the sharp rotations ΔB_y and ΔV_y.

[9] In Figure 2 the ACE data have been delayed by 70 minutes. This delay is approximate and is derived as follows. The Greenland-West Coast magnetometer chain was located at 11:00 magnetic local time (MLT). As shown in Figure 3, which displays a stack plot of the north-south component at five stations, a large disturbance is recorded starting at ~13:55 UT (see station STF), giving a delay from ACE to the ground near noon of 68 min. The inner magnetospheric propagation time from the magnetopause to the ground via MHD waves is typically estimated as 1–3 min, which results in a delay time for the IMF to propagate from ACE to subsolar magnetopause of ~65 min. Further, we consulted the magnetic records of GOES 8 (located at 10:00 MLT at 14:00 UT), Canadian Auroral Network for the OPEN Program (CANOPUS) (at dawn local times), and International Monitor for Auroral Geomagnetic Effects (IMAGE; at ~17:00 MLT at 14:00 UT). All show a large response starting at about 13:58 UT ± 3 min. Given that the impact point (see below) is at midafternoon local times, this should also give the approximate delay to Cluster, for which we shall henceforth assume a delay time of 70 min.

3. Cluster Observations at the Magnetopause

[10] For the observations at the magnetopause we shall focus on Cluster 3 data. The Cluster suite of spacecraft were on an outbound trajectory just tailward of the dusk terminator and at northern latitudes. (At this early stage of the mission, the spacecraft separation was of the order of a few hundred km and all spacecraft see the same features.) At 14:00 UT the location of Cluster 3 in GSM coordinates was (−2.4, 13.2, 6.3) R_E and it is at a magnetic local time of 18:13 and 26.7° magnetic latitude. For some hours prior to our observations, the spacecraft stayed in the vicinity of the magnetopause because the magnetopause boundary was expanding slowly outward because of a slow decrease in dynamic pressure. The position of Cluster 3 relative to the magnetopause between 13:00 and 15:00 UT on 7 December 2000 is shown in Figure 4, which gives the radial distance D_r of the spacecraft from the model magnetopause of *Shue et al.* [1998]. In this model, the time profiles of the solar wind parameters $P_{\rm dyn}$ and B_z enter as inputs, and therefore the model takes account of two major interplanetary parameters affecting the shape and size of the magnetosphere. From 14:00 to 14:30 UT the spacecraft stays within a distance of 0.4 R_E from the magnetopause. We may reasonably assume that Cluster 3 is inside the boundary layer according to the model, which is in agreement with instrument readings discussed shortly. The short and long horizontal bars indicate the times when two periodic perturbations of different amplitude and period were observed, starting at 13:58 UT, about the estimated time of

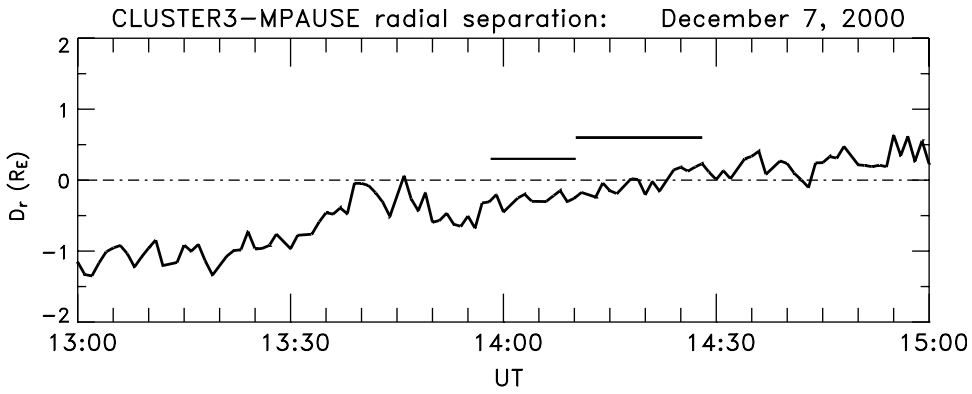

Figure 4. The radial distance of Cluster 3 (D_r) from the model magnetopause of *Shue et al.* [1998]. Negative values of D_r indicate positions earthward of the model magnetopause. The short and long horizontal bars indicate the intervals during which oscillatory motions of different periods were observed by Cluster.

arrival of the joint discontinuity at Cluster. Not taking into account transient motions this model predicts for the prevailing conditions a shape factor, i.e., the ratio of the distance to the terminator to that to the subsolar point, of 1.56 for the period shown in the Figure 4.

[11] Figure 5 shows Cluster 3 observations for the time period 13:55–14:30 UT around the time of the TD/VS impact. From top to bottom, Figure 5 displays the density, proton temperature, components of the field and flow in GSM coordinates, and total field and bulk flow. The data are from the Cluster Ion Spectrometry (CIS) [*Rème et al.*, 1997] and FluxGate Magnetometer (FGM) instruments [*Balogh et al.*, 1997], respectively, plotted at 4-s spin resolution. From ~13:58 to ~14:10 UT four large oscillations are recorded, particularly striking in the proton temperature and density variations. They are accompanied by changes in the field and flow. The period of these oscillations is ~3 min. These large oscillations then die out, and from about 14:10 to 14:28 UT another type of undulatory motion, of a shorter period, becomes evident, being this time particularly conspicuous in the fluctuations in the GSM components of the magnetic field, polarity reversals in B_x and B_y, and quasi-periodic variations in the plasma velocity. Simultaneously, the strength of the total field and flow are subject to large changes. The period of these motions is ~79 s (12.6 mHz), as also established below when examining power spectra. A closer examination shows that the fluctuation level (see for example B_z) is in general stronger in the period ~14:10–~14:20 than in the period ~14:20–~14:28 UT. This point is discussed in section 4.2.

[12] Figure 6 displays H^+ spectrograms for the same period from Cluster 3. Differential energy fluxes are plotted against time, with intensities color coded according to the color bar on the right. Up to 14:10 UT the CIS instrument records the alternate presence of high- and low-energy hydrogen ions. These correspond to the large oscillations. In each cycle, brief, relative depletions of high-energy particle fluxes alternate with relative depletions of low-energy particle fluxes. It appears that the magnetopause/boundary layer is performing large in-and-out excursions at whose extremities the spacecraft samples the magnetosheath and the magnetospheric plasma. By contrast, the most striking feature in the 14:10–14:20 UT time interval is that the low-energy population is always present at high intensities, while the high-energy particles are episodically depleted or absent. The average period is now ~80 s. This is consistent with a wave traveling on the boundary, the absence of high energies indicating that the spacecraft is briefly in the magnetosheath, while when both populations are present, it is in the boundary layer. Taking an average bulk speed of ~200 km s^{-1} (Figure 5), we infer a wavelength of ~2.5 R_E. In the time interval 14:20–~14:28 UT, similar features are seen but times when the high-energy population is absent coincide with a relative depletion of the low-energy particles as well (for example, at 14:23 UT). In summary, the arrival of the joint tangential discontinuity/vortex sheet (TD/VS) and its trailing period of the northward IMF excited a two-stage response near the low-latitude dusk meridian. In the next section we offer a possible interpretation of this two-stage response at the magnetopause.

[13] We now estimate the location of the impact point of the TD/VS on the magnetopause. A schematic of the TD/VS approaching the magnetosphere is shown in Figure 7. Assuming for simplicity that its orientation remains unchanged on passing through the bow shock and taking a paraboloidal magnetosphere with the shape factor = 1.56, as inferred from *Shue et al.*'s [1998] model (not shown), with a subsolar distance of 9 R_E (corresponding to a solar wind dynamic pressure of 4 nPa), a simple calculation gives the point of its impact with the magnetopause in GSM coordinates as (7.2, 5.0, −4.4) R_E (GSM). Thus the impact occurs at midafternoon MLTs south of the GSM equator.

[14] The impact of the discontinuity on the magnetopause caused a global effect. On this, we discuss briefly the reading at the CANOPUS magnetometers, which were at dawnside MLTs. Figure 8 shows a stack plot of the north-south components (X, positive north) of the geomagnetic field at seven midlatitude to high-latitude stations from the Churchill line of the CANOPUS magnetometer network (now operating as the Canadian Array for Realtime Investigations of Magnetic Activity (CARISMA), see www.carisma.ca) located at ~08:00 MLT (meridional chain). The records from the various stations are color coded as shown and range over 20° in latitude from ~60° (station PINA) to ~78° (station TALO, numbers quoted in corrected geomag-

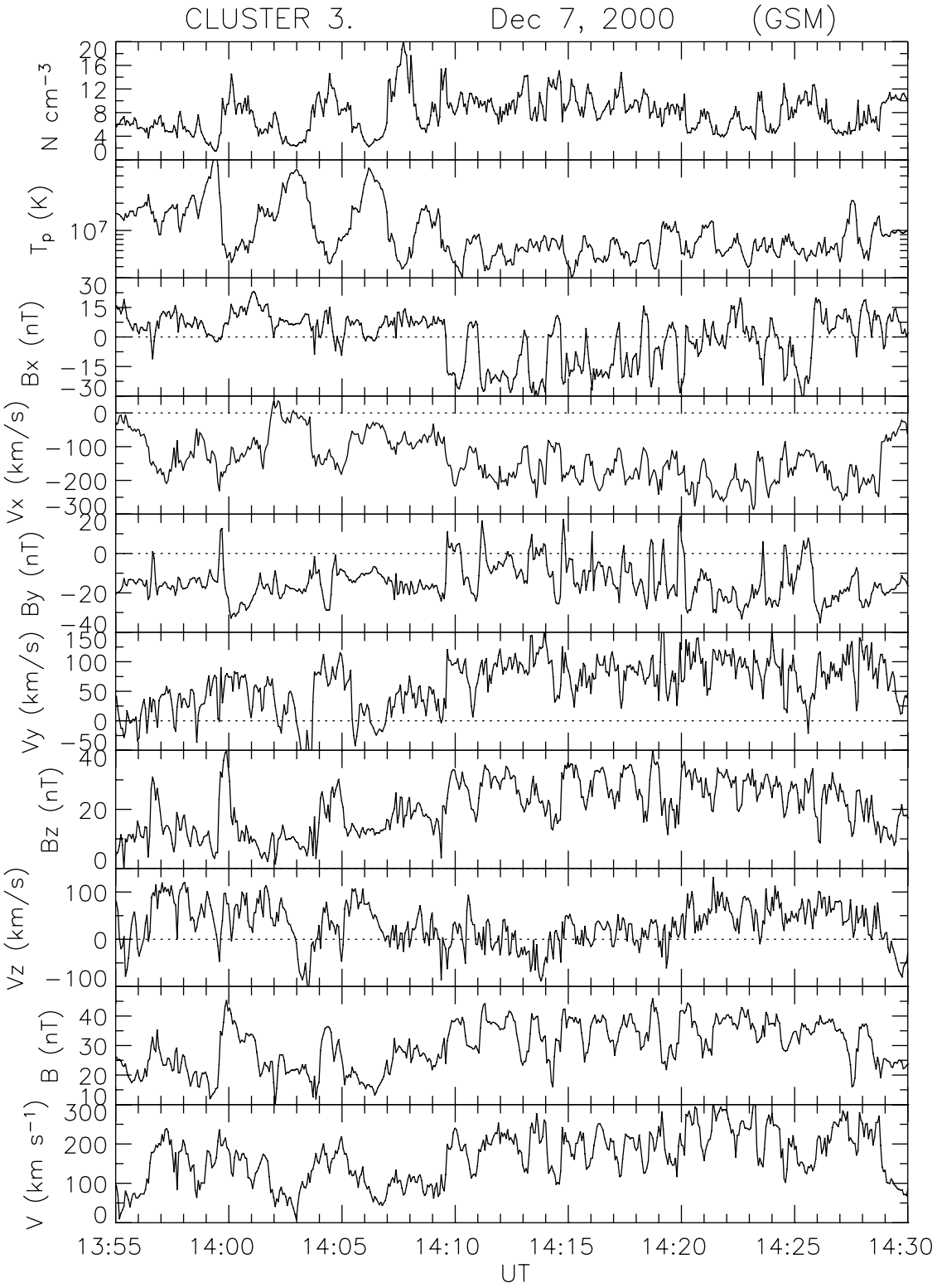

Figure 5. Cluster/CIS and FGM data from Cluster 3 for the time interval 13:55–14:30 UT: the proton density, temperature, components (pairwise) of the magnetic field and plasma flow vectors, total field, and bulk speed.

netic coordinates). Clearly, the response depends on magnetic latitude. A transient, oscillatory response is evident at stations GILL, ESKI, and RANK. A change of phase occurs between stations FCHU and ESKI, indicating a resonance at $\sim$69° corrected geomagnetic latitude. The oscillatory signal is damped and at 08:00 MLT has a comparable period to that observed at Cluster ($\sim$3.2 min at station GILL). In these respects, although excited by tangential stresses as we show

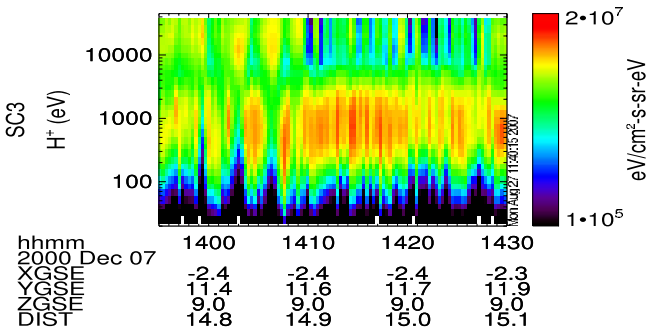

Figure 6. Differential energy fluxes of H^+ from the Cluster 3 spacecraft for the interval 13:55–14:30 UT. The intensities are as indicated by color bar on the right.

below, the effect of magnetopause motions are similar to the geomagnetic ULF pulsations excited inside the magnetospheric cavity by motions of the magnetopause driven by changes in the dynamic pressure [*Farrugia et al.*, 1989].

[15] Figure 9 shows now a longitudinal chain (i.e., approximately at the same latitude) of ground stations from the CANOPUS array. Plotted are the records from stations DAWS, FSMI, and GILL, lying within a latitudinal band of 3° around 66°. The oscillations are seen only on GILL, situated at ~08:00 MLT, and FSMI, situated further tailward at 06:00 MLT. The transition from the background fluctuations into a coherent oscillatory motion starts abruptly at both stations but it occurs ~2.5 min earlier at GILL than at FSMI, indicating a tailward propagation of the disturbance (see vertical arrows). From the different onset times at GILL and FSMI we infer a meridional velocity component of the disturbance on the ground of ~9 km s^{-1} at the average geomagnetic latitude of the stations (~65°). The period is longer at the earlier (in MLT) station by a factor of 1.16 (horizontal arrows), suggesting that the phase speed of the ionospheric disturbance increases as it propagates antisunward.

4. Analysis/Interpretation

4.1. Stage 1: Large-Amplitude Motions of the Magnetopause

[16] We discuss first the cause of the large amplitude motions of the magnetopause. As noted, ACE observations show only a ~17% rise in dynamic pressure, but there is also a large change in the east-west component of the flow V_y (section 2). With the work of *Zong et al.* [2004] in mind (see section 1), we now look at the off-diagonal elements of the total pressure tensor.

[17] The total pressure tensor (total momentum flux tensor) is given by

$$\Pi_{\alpha\beta} = \left(p + \frac{B^2}{2\mu_0}\right)\delta_{\alpha\beta} + \rho V_\alpha V_\beta - \frac{B_\alpha B_\beta}{\mu_0},$$

where α and β are running indices. Using the TD/VS coordinates i, j, k (Figure 2) with $B_k = 0$, the component of momentum flux normal to the discontinuity plane is

$$\Pi_{kk} = \rho V_k^2 + p + \frac{\left(B_i^2 + B_j^2\right)}{2\mu_0}.$$

[18] Note that at the moment of impact, vector **k** is normal to both the discontinuity as well as to the magnetopause, so that Π_{kk} represents the pressure normal to the boundary. The components of the momentum flux in the TD/VS plane are

$$\Pi_{k\beta} = \rho V_k V_\beta,$$

where $\beta = i, j$ and their variation across the discontinuity plane is important.

[19] Figure 10 plots from top to bottom the B_i component of the IMF for reference, quantity P_{kk} ($\equiv \rho V_k^2 + p$) and Π_{kk} (red trace), followed by Π_{ki}, and Π_{kj}. It is clear from the second panel that the magnetic tension forces are negligible for these considerations. Taking 5-min averages on either side of the discontinuity we then have $\Delta\Pi_{kk} = 0.18$ nPa (normal pressure), $\Delta\Pi_{ki} = -0.45$ nPa, and $\Delta\Pi_{kj} = 0.31$ nPa for the tangential stresses. Thus the total jump in the tangential stress, i.e., $\sqrt{((\Delta\Pi_{ki})^2 + (\Delta\Pi_{kj})^2)} = 0.55$ nPa, which is a factor of about 3 larger than the change in the normal pressure. We conclude that the ~3-min oscillations of the magnetopause in the early part of the period were mainly brought about by a change in the tangential stresses, i.e., the vortex sheet aspect of the discontinuity played a substantial role, much more significant than that of the dynamic pressure.

4.2. Stage 2: Kelvin-Helmholtz Instability

[20] We carried out a stability analysis of a limited segment of the magnetopause, where the boundary layer may be considered to lie in a local tangent plane. The boundary layer is then modeled as a planar plasma slab with stratified density, flow velocity, and magnetic field. The study is done with a numerical code that solves the linearized compressible, ideal MHD equations for KH perturbations.

[21] We first introduce a local Cartesian coordinate triad: the unperturbed boundary layer extends in the y direction normal to the magnetopause (MP) and is uniform over planes of constant y, so that physical quantities do not depend on the coordinates x, z. Since the flow velocity

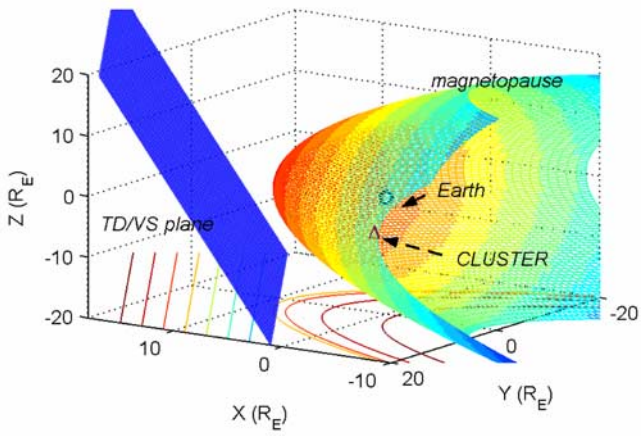

Figure 7. Schematic showing the TD/VS approaching the magnetopause. The position of Cluster is indicated.

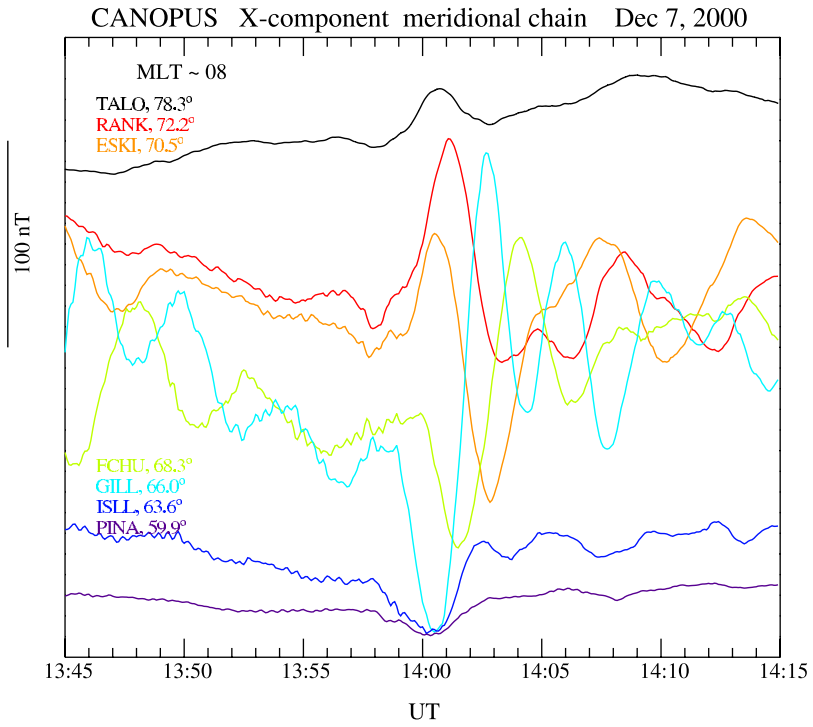

Figure 8. The geomagnetic field at dawn as recorded by a meridional chain of stations from the Churchill line of the CANOPUS magnetometer network situated at ~08:00 MLT. The station latitudes are quoted in corrected geomagnetic latitudes. A resonance is indicated between the latitudes of stations ESKI and FCHU.

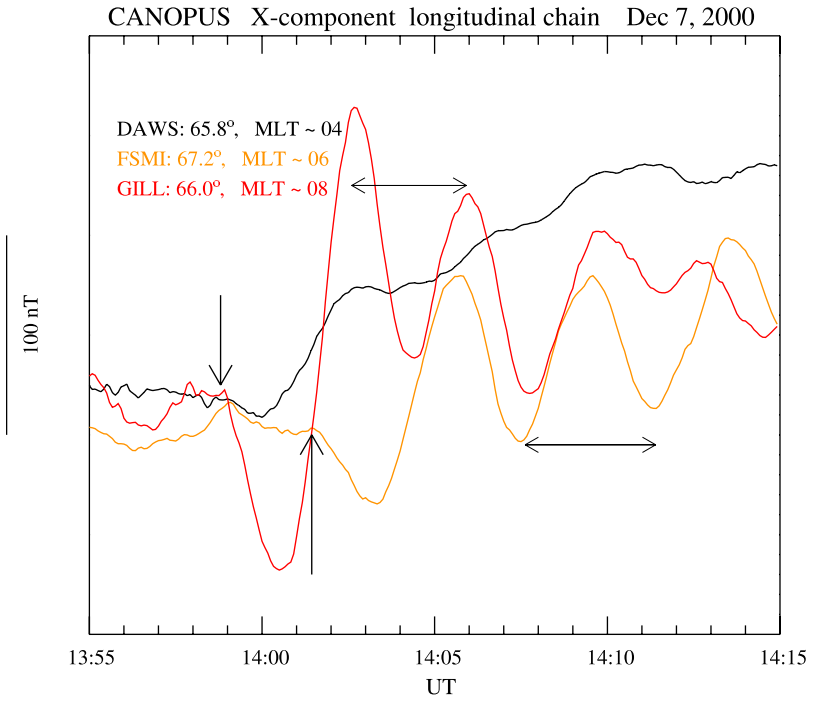

Figure 9. As in Figure 8 but this time for a longitudinal chain (approximately constant latitude). Note the antisunward propagation of the ionospheric disturbance. For more details, see text.

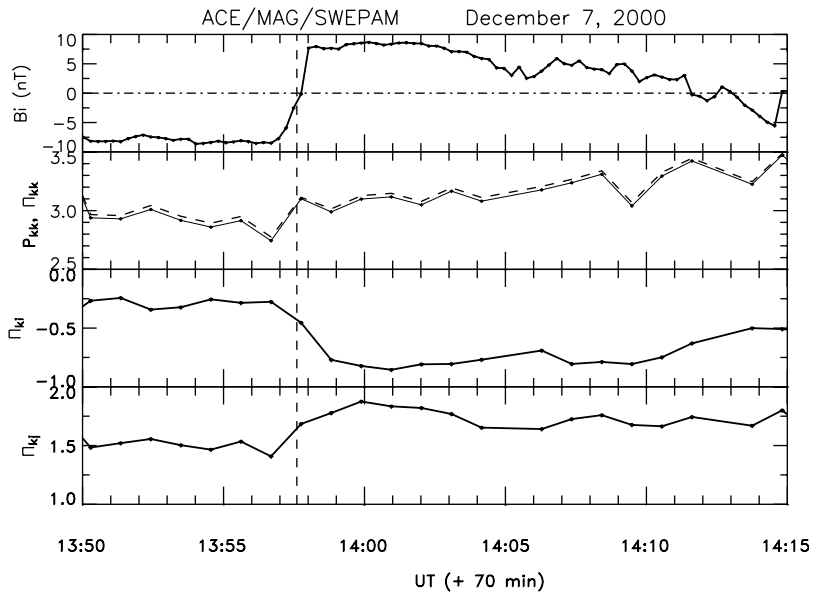

Figure 10. Elements of the total pressure tensor. The first panel reproduced B_i for reference. Then follows the plasma pressure normal to the magnetopause at the TD/VS impact (solid), augmented by the magnetic tension (dashed) and the tangential stresses on the magnetopause in the *i*th (P_{ki}) and *j*th (P_{kj}) directions.

does not change direction as y varies, i.e., across the boundary layer (parallel flow), it is convenient to align the x axis with the mean bulk velocity **V**. The magnetic field **B**, instead, ordinarily changes in both direction as well as strength across the boundary layer. The initial unperturbed model is then represented by the following vector and scalar fields, $\mathbf{V} = (V_x(y), 0, 0)$, $\mathbf{B} = (B_x(y), 0, B_z(y))$, $\rho(y) = m_p n(y)$, and $T(y)$ (where ρ is the mass density and m_p is the proton mass).

[22] The MHD perturbation of the system is described by Fourier modes of the type

$$\Xi = \zeta(y)\exp(-i\omega t + ik_x x + ik_z z), \tag{1}$$

where Ξ is the y component of the Lagrangian displacement of a plasma element from the unperturbed position and ζ is its Fourier mode amplitude. From a knowledge of $\zeta(y)$ all other MHD perturbed quantities can be computed. In the Fourier mode the complex-valued angular frequency is denoted by $\omega = \omega_r + i\gamma$; the wave vector is $\mathbf{k} = (k_x, 0, k_z)$, assumed to be a given real quantity; and its modulus k is given by $k^2 = k_x^2 + k_z^2$. The mode amplitude is governed by a second-order differential equation (2) below that leads to a nonlinear boundary problem for the unknown ω, which appears folded in a nonlinear fashion in the equation. The real part ω_r is the angular frequency, and the imaginary part is the growth rate (when $\gamma > 0$) of the Fourier modes (damping rate if $\gamma < 0$).

[23] The perturbed state is governed by the following equation derived from the linearized ideal MHD equations (see *Gratton et al.* [1988] or for an alternative treatment, the reader is referred to *Miura and Pritchett* [1982]).

$$\frac{d}{dy}\left[H\left(1-\frac{1}{M}\right)\frac{d\zeta}{dy}\right] - k^2 H\zeta = 0, \tag{2}$$

in which the functions H and M are defined by

$$H(y) = \rho(y)\left[(c - V_\kappa(y))^2 - V_{A\kappa}^2(y)\right], \tag{3}$$

$$M(y) = 1 - \frac{\left(V_A^2 + c_S^2\right)}{(c - V_\kappa)^2} + \frac{\left(V_{A\kappa}^2 c_S^2\right)}{(c - V_\kappa)^4}. \tag{4}$$

[24] In these expressions V_A is the Alfvèn speed, c_s is the speed of sound, and V_κ and $V_{A\kappa}$ are the projections of **V** and $\mathbf{B}/\sqrt{4\pi\rho}$, respectively, on the **k** direction. (The subscript k in this section should not be confused with the designation k for the normal direction in minimum variance analysis.) All these quantities are functions of y. The important unknown, to be determined from the solution of the problem, is the (complex) phase speed $c = \omega/k = \omega_r/k + i\gamma/k$, whose real part gives the phase velocity of the modes and whose imaginary part is related to their growth (or damping) rate.

[25] The profiles of the fields across the boundary layer are modeled by hyperbolic tangent functions, $\tanh(y/d)$, where d is one-half the scale length $\Delta = 2d$ of the velocity gradient transition. This quantity need not be specified since the results are obtained as normalized quantities. Quantity Δ is related to the width of the boundary layer, represented in this model approximately by $2 \times \Delta$. The asymptotic values of the fields on either side of the transition are joined by functions of y written as a linear combination of a constant and a hyperbolic tangent. In this way the physical parameters that determine the model are the intensities of the vector fields $V = |\mathbf{V}|$ and $B = |\mathbf{B}|$, the values of the scalar fields ρ and T, and the angles between **V** and **B**, given at both sides of the transition. The temperature profile $T(y)$ follows from the previous assumptions on ρ and **B** together with the pressure balance condition across the boundary

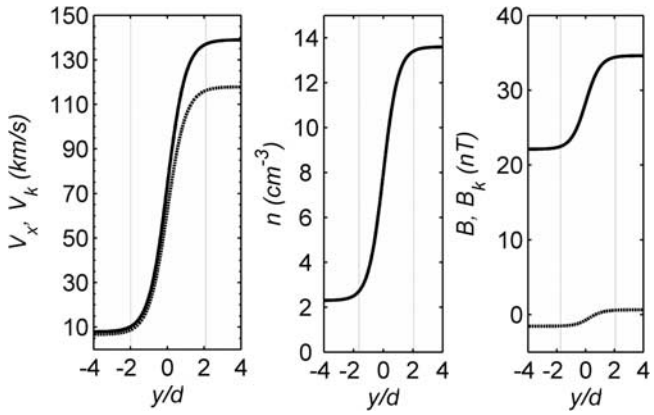

Figure 11. Model profiles of physical quantities across the boundary layer. From left to right: the bulk speed V_x and its projection on the **k** vector V_k, density, and magnetic field strength B and its projection B_k.

layer $p + |\mathbf{B}|^2/8\pi$ = const. The variations of these quantities are shown in Figure 11. Figure 11 shows from left to right: the profiles across the boundary layer of bulk flow V and its projection V_k, density, and magnetic field strength B and its projection on **k**, i.e., B_k. In the projections shown, we used the wave vector direction for the fastest growing mode (see below).

[26] The physical quantities on either side of the magnetosheath-magnetosphere (index 1 and 2, respectively) transition are obtained from the Cluster 3 readings at the extremes of the large oscillations recorded after 13:58 UT. Specifically, we selected the second oscillation, where the lowest speed was recorded at maximum T. That is, we assume that at the extremes of the oscillation, Cluster 3 samples alternately the high-density-low-temperature magnetosheath plasma and the low-density-high-temperature magnetosphere plasma. In this way the local instability is examined by parameters measured locally and in temporal proximity. The input quantities employed in the stability study, i.e., density, magnetic field intensity, temperature, and the angle between field and flow directions, are listed in Table 1 from top to bottom, respectively.

[27] The velocity of the flow on the magnetosheath side U_1 is the reference speed that we use for normalizations. From Table 1 it follows that at the Cluster position, the sonic Mach number (ratio between the plasma velocity and the speed of sound $M = U_1/c_S$) and the Alfvènic Mach number (ratio between the velocity of plasma and the Alfvèn speed $M_A = U_1/V_A$), both conventionally evaluated on the magnetosheath side are $M = 0.40$ and $M_A = 0.68$, respectively. The magnetic shear angle $\delta\theta$ (angular change of direction of the magnetic field across the boundary layer) turns out to be very small ($\sim 5^\circ$). Thus the local magnetic fields on both sides of the boundary are nearly aligned with each other. This property of the local configuration favors the excitation of the KH instability since the stabilizing influence of the magnetic field critically depends on the presence of a substantial magnetic shear angle, which is here much reduced. Thus, while in the present case, where $M_A < 1$, the magnetic tensions are significant, they can be switched off by choosing a direction of the **k** vector normal to **B**. Since the flow is subsonic ($M < 1$), compressibility does not exert a sufficient stabilizing influence, as we shall verify.

[28] The normal modes must approach zero on both sides of the magnetopause, that is, $\zeta \rightarrow 0$ when $y \rightarrow \pm\infty$. However, for a given k, this happens only for particular values of the complex frequency. The boundary value problem that fixes the characteristic value c is then solved numerically by a conventional shooting method (see, for instance, *Keller* [1992]).

[29] Figure 12 plots the growth rate versus k and represents the main result of the stability calculation. It illustrates the change of the growth rate γ of the unstable modes represented by $g \equiv \gamma d/U_1$, as a function of the absolute value of the wave number kd; both quantities are expressed in dimensionless quantities using parameter $d = \Delta/2$. The results are shown for a particular angle between **k** and **V**, i.e., $\varphi = 32^\circ$, corresponding to maximum growth rates. This angle is found by varying the orientation of **k** in the (x, z) plane. The maximum growth rate is given by $\gamma_m = 0.079\ U_1/d$ for a mode with wavenumber $k_m = 0.55/d$. Hence, the mode with fastest growth has a wavelength $\lambda_m \approx 5.7\Delta$.

[30] We now derive an estimate of Δ and τ_e (the e-folding time of the KH instability) by combining this theory with the Cluster measurements. From section 3 the oscillations of period 79 s observed by Cluster correspond to a wavelength of $\approx 2.5\ R_E$. Assuming that this value reflects the wavelength of the fastest KH mode, we infer from $k_m = 0.55/d$, i.e., $\lambda_m \approx 5.7\Delta$, that $\Delta \approx 0.44\ R_E$, giving an estimated boundary layer width of $\approx 0.9\ R_E$. Using this estimate for Δ, the corresponding e-folding time for the growth of the fastest mode is $\tau_e = 1/\gamma \approx 89$ s (a quantity that increases linearly with the estimated Δ value). Since $M_A^2 \approx 0.5$ the magnetic tensions are strong and govern the development of the instability. Thus, as noted above, the most unstable mode has a wave vector **k** oriented nearly perpendicular to the average direction of the magnetic field (magnetosheath and magnetosphere) because the stabilizing influence of the

Table 1. Input Parameters for KH Calculations

14:05 UT	Magnetosheath	14:03	Magnetosphere
n_1	13.6 cm^{-3}	n_2	2.3 cm^{-3}
B_1	34.6 nT	B_2	22.1 nT
U_1	139 km s^{-1}	U_2	$\sim$0 km s^{-1}
T_1	0.38 keV	T_2	$\sim$2.6 keV
$\theta_1(B_1 \angle V)$	121°	$\theta_2(B_2 \angle V)$	126°

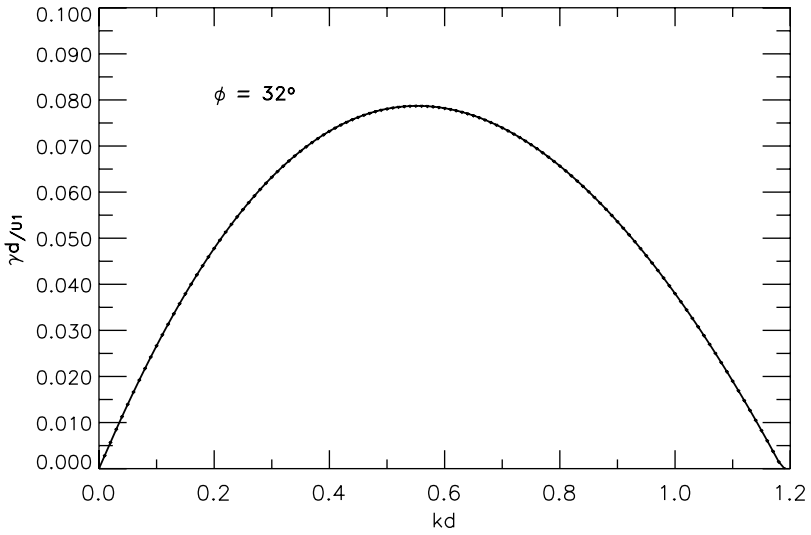

Figure 12. The growth rate, represented by $g \equiv \gamma d/U_1$, as a function of the wave number k. Both quantities are normalized by $d = \Delta/2$, half the length scale of the velocity gradient, and U_1 the velocity of the magnetosheath flow. The angle $\varphi = 32^\circ$ remains fixed and corresponds to the maximum growth rate.

magnetic field is then minimal. In this case it is almost zero, since $\delta\theta \approx 0$.

[31] The oscillations of period ~79 s recorded by Cluster are not present before the large amplitude oscillations induced by the joint discontinuity. They are a consequence of the change of local conditions brought about by the TD/VS arrival. Taking into account the ~70-min ACE-Cluster delay, the decrease of IMF clock angle α recorded at ACE is felt at Cluster after 13:59 UT; it remains at ~45° for about 5 min and then drops further to values close to zero during the next 9 min (~14:03–14:12 UT, Cluster time, when average $\phi \sim 10^\circ$). At the flank site where Cluster is located it produced a substantial decrease of the magnetic shear (as recorded by the large MP excursion from 14:03 to 14:05 UT) and the theory confirms that the region is KH unstable.

[32] A small clock angle is also influential in fostering KH activity on the frontside magnetopause, for reasons explained by *Farrugia et al.* [1998] and *Gratton et al.* [2004]. Therefore, the presence of KH excitation, generated far upstream over the dayside and convected to the flanks by the flow should also be expected.

[33] Looking at Figure 2, ACE records a small clock angle from 14:05–14:12 UT (Cluster time), which averages ~10°. After 12:12 UT, the clock angle increases briefly only to return to small values at 14:17 UT. At 14:20 UT the clock angle increases to ~70° and remains large. Looking now at Figure 5, we see a clear change in the character of the oscillations at Cluster 3, starting at ~14:20 UT; a decreasing trend of amplitudes sets in and continues during 14:20–14:29 UT.

[34] To investigate this change in oscillatory behavior, a spectral analysis of Cluster data was performed. We chose B_z as a representative quantity. We subdivide the interval ~14:10–14:29 UT into two parts: phase I from 14:09:30–14:19:58 UT and phase II from 14:19:58–14:28:45 UT. A running average over eight data points has been carried out to subtract the declining trend in the second interval. A constant background average has been subtracted in the first interval. In Figure 13 the power spectral density corresponding to the two phases (phase I, black line; phase II, red line) show a peak power ratio of 2.9, with practically the same frequency (12.6 versus 13.3 mHz).

[35] We now inquire into the drop in power spectral density during phase II. We hypothesize that the increase in clock angle α (a quantity which remains invariant across the bow shock [*Song et al.*, 1992]) in phase II reduced the remote production from the dayside (in accordance with theory [*Farrugia et al.*, 1998; *Gratton et al.*, 2004]). (By "remote production" we mean growth on the boundary upstream of the point of observation.) Furthermore, through the accompanying reorientation of the magnetosheath field close to the magnetopause the local growth rates at the Cluster region were also reduced. The latter statement can be investigated by theory, using the numerical code for the linear KH instability analysis. Using the values of Table 1, we decrease the local angle between the magnetic field and the flow at the magnetosheath side θ_1 in steps from 121° to 90°, keeping all the other quantities constant. This models a shift of the magnetic field direction, to correspond with the increase in clock angle. As θ_1 decreases from the measured value of 121°, we search for the value of the maximum growth rate mode by changing φ (as before, the angle between the wave vector **k** and the flow direction). We also test for possible changes of the wavelength of the mode, but we find that the value of $kd = 0.55$ for fastest growth does not vary. The results are summarized in Table 2 which shows that a change of 20° in θ_1 reduces the normalized growth rate by a factor of 2.7, while a 30° shift eliminates the local instability altogether.

[36] Finally, an interesting point emerges from this analysis. While the wavelike perturbations appear immediately after the great oscillations (at ~14:10–14:20 UT) in coincidence with the drop in clock angle, a significant growth of the KH instability from small perturbations alone needs a period of several τ_e. For instance, it takes $3.9 \times \tau_e$ for a fiftyfold amplification of a 1% amplitude perturbation. Given the shortest *e*-folding time we have estimated (89 s), ~5.6 min would be required for the amplitude of the mode

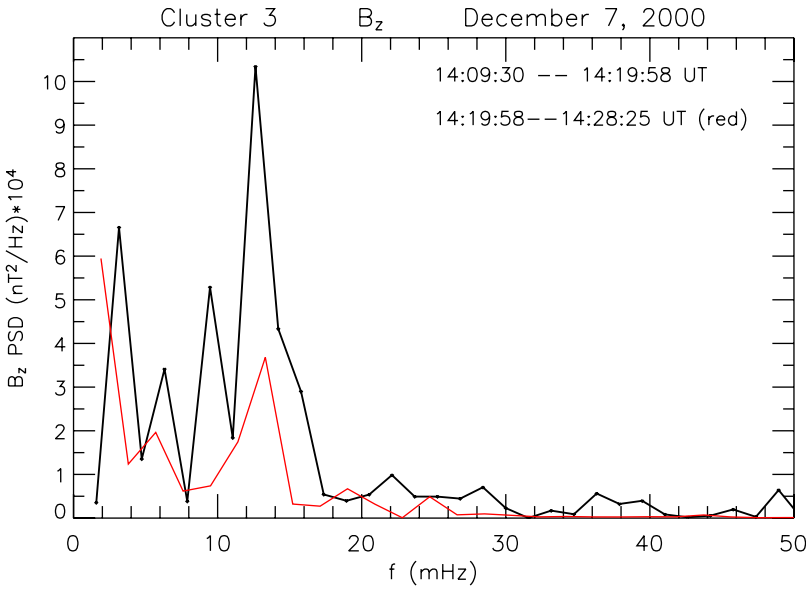

Figure 13. The power spectral density of the fluctuation in B_z. The black line refers to the period 14:09:30–14:19:58 UT, while the red line refers to 14:19:58–14:28:45 UT.

to grow from noise to a significant level. The conclusion is that the preceding large oscillations (~13:59–14:09 UT) have, in some way, shortened the development of the KH instability. It appears that the general perturbation of the MP caused by the TD/VS arrival adds to the fluctuation level already present in the low-latitude boundary layer and has accelerated the evolution of the KH process. We conjecture that the TD/VS impact on the magnetopause tripped the instability, as happens to classic fluid dynamic flows when subject to strong perturbations.

5. Discussion and Conclusions

[37] We have elaborated a case study where a well-defined interplanetary field and flow discontinuity followed by an interval of northward IMF gave rise first to a burst of coherent 3-min period large-amplitude deformations of the magnetopause, which propagated as waves along the boundary, and were then succeeded by a burst of Kelvin-Helmholtz surface waves of ~79 s period. The interplanetary structure had some pleasing properties from a space plasma physics point of view. Large and sharp rotations of the east-west component of both field and flow took place at constant field strength and approximately constant bulk speed and plasma density. This allowed its effects on the terrestrial field and plasma environment to be isolated and studied. Though we placed emphasis on the magnetopause, we also found that the effect of the tangential stresses exerted during the TD/VS impact had a global character, affecting geomagnetic field and plasmas over at least 12 h of magnetic local time.

[38] By virtue of these properties, but most importantly the almost constant density, the interaction of this combined tangential discontinuity/vortex sheet with the bow shock is not complicated by the generation of subsidiary MHD waves and readjustments of the shock location. *Wu et al.* [1993] simulated the interaction of the bow shock with interplanetary tangential discontinuities. This can be quite complex and involves the creation of MHD wave modes (fast and rarefaction waves), which propagate toward the magnetopause ahead of the original discontinuity, and the strengthening or weakening of the bow shock, depending on the sign of the density change. From that analysis it emerged that the key parameter controlling the strength of this interaction is the change in solar wind density at the discontinuity. Wu et al. worked with a factor of 2 change (increase or decrease), whereas we had only a ~9% increase. They showed that the effects became minimal when this change decreases, and the effect is further weakened when the magnetic field strength does not vary across the discontinuity. From these factors we therefore conclude that the discontinuity we examined is little affected when passing through the bow shock except that the coplanarity plane of the shock is changed. A further nice property is that, as *Wu et al.* [1993] point out, a change in magnetic field and flow direction are maintained across the bow shock and have no effect on the interaction. All these properties make the study of such a structure a very instructive exercise. (The reader is also referred to *Kauristie et al.* [2001], who examined other aspects of this event.)

[39] The analysis allowed us to add to the gathering evidence that sharp rotations in the azimuthal component of the solar wind velocity is important in exciting motions

Table 2. Growth Rates Resulting From a Variation of the Local Angle of Magnetic Shear

θ_1	φ_1	$\gamma d/U_1$
121°	32°	0.079
110°	25°	0.063
100°	17°	0.029
90°	10°	0.000

of magnetospheric boundaries. The location of the cusp was highlighted in previous work (see section 1); here we focussed rather on the magnetopause. The tangential pressure tensor elements were important in our case and it is mainly these which gave rise to the magnetopause deformations.

[40] What role did ΔB_y play in our example? Two roles are clear: (1) it defined the discontinuity and (2) it affected the IMF clock angle, and thence the local magnetic shear across the magnetopause at the dusk terminator where Cluster was located. This turned out to be small after the arrival of the TD/VS, favoring the development of Kelvin-Helmholtz activity. In addition to these two roles, the rotation in B_y enters, of course, in the stress tensor components. We calculated these, but found the effect of magnetic tension in the normal stresses applied to be minimal.

[41] In section 1 we mentioned work which addressed another effect of IMF B_y changes on the position of magnetospheric boundaries. Variations of the IMF orientation can produce pressure variations in the foreshock region which then affect the magnetopause. The controlling influence was found in these studies to be the angle between the bow shock normal and the direction of the IMF θ_{nB}, and the effects are more pronounced behind a parallel bow shock (at dawn, in our case). In our analysis we did not find the effects of foreshock-produced pressure variations. It may be they were present but were masked by the large oscillations of the whole boundary. We point out, however, that there was a background oscillatory noise prior to and after the interval we study (Figures 8 and 9). It is unclear to us where this comes from, but we do not exclude that it may be due to just this effect of the IMF B_y rotation.

[42] In studying the KH surface waves, we profited from the fact that close in time and space the magnetosphere and magnetosheath plasmas were sampled during the large excursions of Cluster as the magnetopause oscillates over the spacecraft. Thus the boundary conditions for the KH analysis are set well.

[43] The KH stability at the Cluster position was analyzed by a theoretical model and instability was confirmed. We could distinguish two phases in the KH activity in the Cluster data: a strong phase (phase I) was followed by one where the frequency was unaffected but the power spectral density was much reduced (phase II). We argue that the changes in the clock angle recorded by ACE were responsible for this. We examined the instability theoretically and showed, in fact, that under reasonable assumptions on the effect of the clock angle on the local magnetic shear, the magnetopause configuration became stabilized locally during the second phase. That the activity persisted, albeit at a much reduced rate, is presumably also because KH waves are still arriving from destabilized regions farther upstream on the dayside. We note that *Kauristie et al.* [2001] also suggested the presence of KH activity.

[44] Work on KH instability at the magnetopause is important because this instability is one of the possible mechanisms which have been invoked to explain plasma entry when IMF B_z points northward. One recent context concerns the long (several hours) intervals when the plasma sheet is found to be cold and dense; the early reports coming from Geotail observations [*Fujimoto et al.*, 1996, 1998; *Terasawa et al.*, 1997] having been since repeatedly confirmed. Cold, dense plasma sheets are currently being intensely studied. The role of KH in their formation is much debated and is considered as a competing mechanism to plasma entry via reconnection poleward of the cusp [see, e.g., *Thomsen et al.*, 2003; *Øieroset et al.*, 2005, and references therein].

[45] The effect on the magnetopause/magnetosphere of the tangential stresses resemble those induced by normal dynamic pressure changes. In the context of a search for ionospheric signatures of flux transfer events, *Farrugia et al.* [1989] and *Freeman et al.* [1990] studied magnetopause motions driven directly by large impulsive changes in P_{dyn} (see also *Friis-Christensen et al.* [1988]). The magnetopause motions were analyzed by timing crossings made by two well-separated spacecraft in the magnetopause region (ISEE 1 and 2). In that study it was found that the response on ground magnetometers was latitude dependent, giving rise to both transients (oscillations, which were localized in latitudes) and compressions/rarefactions at other latitudes. A tailward motion of the ground disturbances was also inferred. The transients, which in some stations continued for a few cycles, were excited on resonant L shells when the compressional wave from the outer magnetosphere couples to field-guided Alfvèn waves at L shells (field lines) with matching frequency, setting up standing waves on the field lines. The observed short disturbances at stations not in resonance were caused by shear flows generated locally in the ionosphere which were directly driven by the Alfvèn mode from the high-latitude compression [*Kivelson and Russell*, 1995, chapter 11]. The global nature of the effects was also suggested in these studies, but the availability of ground data at that time allowed the authors to examine only the afternoon side of the magnetosphere. Here the effects were present in ground magnetometer data from dusk, near-noon, and dawn (a 12-h MLT span).

[46] In conclusion, we have elaborated the response of the magnetosphere boundary layer to a joint tangential discontinuity/vortex sheet. Two interplanetary triggers separated in time were involved and, correspondingly, the response consisted of two successive stages. The first trigger, reflecting the vortex sheet aspect of the discontinuity, was the tangential stress associated with an abrupt change in the east-west component of the solar wind flow vector. This turned out to be substantially larger than the change in the normal pressure. The result was to excite large oscillations of the boundary of a ~3-min period. A global response of the magnetosphere was established from ground magnetometer records spread over more than 12 h of local time. It resembled that which previous studies have associated with the application of a variable normal pressure to the magnetopause. Thus magnetosphere dynamics was driven from its magnetopause boundary. The second trigger is an interval of northward-pointing IMF following the TD/VS arrival. Compressible MHD calculations showed that the duskside magnetopause, where Cluster was situated, became Kelvin-Helmholtz unstable, generating surface waves of period ~79 s. The KH activity itself was subdivided into two intervals, with the power spectral density of the fluctuations decreasing markedly in the second, while remaining peaked at the same frequency. The weakening of KH activity occurred when the IMF rotated away from the northward direction. This reorientation stabilized the duskside flank

which, however, kept receiving KH waves generated further to the dayside.

[47] **Acknowledgments.** F.T.G. is grateful for the hospitality at the Space Science Center of UNH, where part of this research was done. Work at UNH is supported by UNH Cluster grant, Cluster-Specific Theory and Modelling grant, and by NASA grant NNG05GG25G. F.T.G., L.B., and G.G. are supported by CONICET grant PIP 5291/05 and UBACYT grant X291/04. The CANOPUS magnetometer array, now operated as CARISMA (www.carisma.ca), was funded by the Canadian Space Agency.

[48] Zuyin Pu thanks Patrick T. Newell and another reviewer for their assistance in evaluating this manuscript.

References

Balogh, A., et al. (1997), The Cluster magnetic field investigation, *Space Sci. Rev.*, *79*, 65.

Chen, S.-H., M. G. Kivelson, J. T. Gosling, R. J. Walker, and A. J. Lazarus (1993), Anomalous aspects of magnetosheath flow and of the shape and oscillations of the magnetopause during an interval of strongly northward interplanetary magnetic field, *J. Geophys. Res.*, *98*(A4), 5727.

Dungey, J. W. (1955), Electrodynamics of the outer atmospheres, *Rep. 69*, Ionos. Res. Lab., Pa. State Univ., University Park.

Fairfield, D. H., W. Baumjohann, G. Paschmann, H. Lühr, and D. G. Sibeck (1990), Upstream pressure variations associated with the bow shock and their effects on the magnetosphere, *J. Geophys. Res.*, *95*(A4), 3773.

Fairfield, D. H., A. Otto, T. Mukai, S. Kokubun, R. P. Lepping, J. T. Steinberg, A. J. Lazarus, and T. Yamamoto (2000), Geotail observations of the Kelvin-Helmholtz instability at the equatorial magnetotail boundary for parallel northward fields, *J. Geophys. Res.*, *105*(A9), 22,159.

Farrugia, C. J., M. P. Freeman, S. W. H. Cowley, D. J. Southwood, M. Lockwood, and A. Etemadi (1989), Pressure-driven magnetopause motions and attendant response on the ground, *Planet. Space Sci.*, *37*, 589.

Farrugia, C. J., et al. (2000), Coordinated Wind, Interball/tail, and ground observations of Kelvin-Helmholtz waves at the near-tail, equatorial magnetopause at dusk: January 11, 1997, *J. Geophys. Res.*, *105*(A4), 7639.

Farrugia, C. J., F. T. Gratton, and R. Torbert (2001), Viscous-type processes in the solar wind-magnetosphere interaction, *Space Sci. Rev.*, *95*(1–2), 443.

Freeman, M. P., C. J. Farrugia, S. W. H. Cowley, D. J. Southwood, M. Lockwood, and A. Etemadi (1990), The response of the magnetosphere-ionosphere system to solar wind dynamic pressure variations, in *Physics of Magnetic Flux Ropes*, *Geophys. Monogr. Ser.*, vol. 58, edited by C. T. Russell, E. R. Priest, and L. C. Lee, pp. 611–618, AGU, Washington, D. C.

Friis-Christensen, E., M. McHenry, C. Clauer, and S. Vennerstrøm (1988), Ionospheric traveling convection vortices observed near the polar cleft: A triggered response to sudden changes in the solar wind, *Geophys. Res. Lett.*, *15*(3), 253.

Fujimoto, M., A. Nishida, T. Mukai, Y. Saito, T. Yamamoto, and S. Kokubun (1996), Plasma entry from the flanks of the near-Earth magnetotail: Geotail observations in the dawnside LLBL and the plasma sheet, *J. Geomagn. Geoelectr.*, *48*, 711.

Fujimoto, M., T. Terasawa, T. Mukai, Y. Saito, T. Yamamoto, and S. Kokubun (1998), Plasma entry from the flanks of the near-Earth magnetotail: Geotail observations, *J. Geophys. Res.*, *103*, 4391.

Gratton, J., A. G. González, and F. T. Gratton (1988), Convective instability of internal modes in accelerated compressible plasmas, *Plasma Phys. Controlled Fusion*, *30*, 435.

Gratton, F. T., L. Bender, C. J. Farrugia, and G. Gnavi (2004), Concerning a problem on the Kelvin-Helmholtz stability of the thin magnetopause, *J. Geophys. Res.*, *109*, A04211, doi:10.1029/2003JA010146.

Kauristie, K., et al. (2001), Ground-based and satellite observations of high-latitude auroral activity in the dusk sector of the auroral oval, *Ann. Geophys.*, *19*, 1683.

Keller, H. B. (1992), *Numerical Methods for Two-Point Boundary-Value Problems*, Dover, Mineola, N.Y.

Kivelson, M. G. and S.-H. Chen (1995), The Magnetopause: Surface Waves and Instabilities and Their Possible Dynamical Consequences, in *Physics of the Magnetopause*, *Geophys. Monogr. Ser.*, vol. 90, edited by P. Song, B. U. Ö. Sonnerup, and M. F. Thomsen, pp. 257–268, AGU, Washington, D. C.

Kivelson, M. G., and C. T. Russell (Eds.) (1995), *Introduction to Space Physics*, Cambridge Univ. Press, New York.

Kivelson, M. G., and D. J. Southwood (1986), Coupling of global magnetospheric MHD eigenmodes to field line resonances, *J. Geophys. Res.*, *91*, 4345.

Laakso, H., et al. (1998), Oscillations of magnetospheric boundaries driven by IMF rotations 1998, *Geophys. Res. Lett.*, *25*(15), 3007.

Lundin, R., B. Aparcio, and M. Yamauchi (2001), On the solar wind flow control of the polar cusp, *J. Geophys. Res.*, *106*(A7), 13,023.

McComas, D. J., et al. (1998), Solar Wind Electron, Proton, and Alpha Monitor (SWEPAM) for the Advanced Composition Explorer, *Space Sci. Rev.*, *86*, 563.

Miura, A. (1984), Anomalous transport by magnetohydrodynamic Kelvin-Helmholtz instabilities in the solar wind-magnetosphere interaction, *J. Geophys. Res.*, *89*(A2), 801.

Miura, A., and P. L. Pritchett (1982), Nonlocal stability analysis of the MHD Kelvin-Helmholtz instability in a compressible plasma, *J. Geophys. Res.*, *87*(A9), 7431.

Moen, J., H. C. Carlson, and P. E. Sandholt (1999), Continuous observation of cusp auroral dynamics in response to an IMF B_y polarity change, *Geophys. Res. Lett.*, *26*(9), 1243.

Newell, P. T., C.-I. Meng, D. G. Sibeck, and R. Lepping (1989), Some low-altitude dependencies on the interplanetary magnetic field, *J. Geophys. Res.*, *94*(A7), 8921.

Øieroset, M. J., J. Raeder, T. D. Phan, S. Wing, J. P. McFadden, W. Li, M. Fujimoto, H. Rème, and A. Balogh (2005), Global cooling and densification of the plasma sheet during an extended period of purely northward IMF on October 22–24, 2003, *Geophys. Res. Lett.*, *32*(12), L12S07, doi:10.1029/2004GL021523.

Otto, A., and D. H. Fairfield (2000), Kelvin-Helmholtz instability at the magnetotail boundary: MHD simulation and comparison with Geotail observations, *J. Geophys. Res.*, *105*(A9), 21,175.

Rème, H., et al. (1997), The Cluster Ion Spectrometry (CIS) experiment, *Space Sci. Rev.*, *79*(1–2), 303.

Seon, J., L. A. Frank, A. J. Lazarus, and R. P. Lepping (1995), Surface waves on tailward flanks of the Earth's magnetopause, *J. Geophys. Res.*, *100*(A7), 11,907.

Shue, J.-H., et al. (1998), Magnetopause location under extreme solar wind conditions, *J. Geophys. Res.*, *103*(A8), 17,691.

Smith, C. W., et al. (1998), The ACE magnetic fields experiment, *Space Sci. Rev.*, *86*, 613.

Song, P., C. T. Russell, and M. F. Thomsen (1992), Slow mode transition in the front side magnetosheath, *J. Geophys. Res.*, *97*(A6), 8295.

Sonnerup, B. U. Ö., and L. J. Cahill Jr. (1967), Magnetopause structure and attitude from Explorer 12 observations, *J. Geophys. Res.*, *72*, 171.

Southwood, D. J. (1979), Magnetopause Kelvin-Helmholtz instability, paper presented at Magnetospheric Boundary Layers Conference, Eur. Space Agency, Paris.

Southwood, D. J., and M. G. Kivelson (1990), The magnetohydrodynamic response of the magnetospheric cavity to changes in solar wind pressure, *J. Geophys. Res.*, *95*(A3), 2301.

Terasawa, T., et al. (1997), Solar wind control of density and temperature of the near-Earth plasma sheet: WIND-GEOTAIL collaboration, *Geophys. Res. Lett.*, *24*, 935.

Thomsen, M. F., J. E. Borovsky, R. M. Skoug, and C. W. Smith (2003), Delivery of cold, dense plasma sheet material into the near-Earth region, *J. Geophys. Res.*, *108*(A4), 1151, doi:10.1029/2002JA009544.

Wu, B. H., M. E. Mandt, L. C. Lee, and J. K. Chao (1993), Magnetospheric response to solar wind dynamic pressure variations: Interaction of interplanetary tangential discontinuities with the bow shock, *J. Geophys. Res.*, *98*(A12), 21,297.

Zong, Q.-G., T. A. Fritz, H. Zhang, A. Korth, P. W. Daly, M. W. Dunlop, K.-H. Glassmeier, H. Rème, and A. Balogh (2004), Triple cusps observed by Cluster: Temporal or spatial effect?, *Geophys. Res. Lett.*, *31*, L09810, doi:10.1029/2003GL019128.

L. Bilbao, G. Gnavi, and F. T. Gratton, Instituto de Fisica del Plasma, CONICET and University of Buenos Aires, Pabellon I, Ciudad Universitaria, C1428EHA Buenos Aires, Argentina. (faustogratton@infip.org)

S. W. H. Cowley, Deptartment of Physics and Astronomy, University of Leicester, University Road, Leicester LE1 7RH, UK.

C. J. Farrugia, L. Kistler, E. Lund, C. Mouikis, C. W. Smith, and R. B. Torbert, Space Science Center, University of New Hampshire, Durham, NH 03824, USA. (farrugia@tweedledee.sr.unh.edu)

I. R. Mann, Avadh Bhatia Physics Laboratory, Department of Physics, University of Alberta, Edmonton, AB, Canada T6G 2J1.

P. E. Sandholt, Department of Physics, University of Oslo, Oslo N-0317, Norway.

H. J. Singer, NOAA Space Environment Center, 325 Broadway Street, Boulder, CO 80305, USA.

J. F. Watermann, Geomagnetism and Space Physics Program, Danish Meteorological Institute, Lyngbyvej 100, Copenhagen, DK-2100, Denmark.